Journal of the Korean Astronomical Society
54: 1 ∼ 8, 2021 February

https://doi.org/10.5303/JKAS.2021.54.1.1
pISSN: 1225-4614 · eISSN: 2288-890X
http://jkas.kas.org

X-ray Properties of the Pulsar PSR J0205+6449 in 3C 58

Minjun Kim and Hongjun An

Department of Astronomy and Space Science, Chungbuk National University, Cheongju 28644, Republic of Korea;
ieha111@chungbuk.ac.kr, hjan@chungbuk.ac.kr

Received August 10, 2020; accepted December 24, 2020

Abstract: We report X-ray timing and spectral properties of the pulsar PSR J0205+6449 measured using *NuSTAR* and *Chandra* observatories. We measure the pulsar's rotation frequency $\nu = 15.20102357(9)\,\mathrm{s}^{-1}$ and its derivative $\dot{\nu} = -4.5(1) \times 10^{-11}\,\mathrm{s}^{-2}$ during the observation period, and model the 2–30 keV on-pulse spectrum of the pulsar with a power law having a photon index $\Gamma_{\rm psr} = 1.07 \pm 0.16$ and a 2–30 keV flux $F_{2-30\ \rm keV} = 7.3 \pm 0.6 \times 10^{-13}\,\mathrm{erg\,cm^{-2}\,s^{-1}}$. The *Chandra* 0.5–10 keV data are analyzed for an investigation of the pulsar's thermal emission properties. We use thermal and non-thermal emission models to fit the *Chandra* spectra and infer the surface temperature T_∞ and luminosity $L_{\rm th}$ of the neutron star to be $T_\infty = 0.5 - 0.8$ MK and $L_{\rm th} = 1 - 5 \times 10^{32}$ erg s^{-1}. This agrees with previous results which indicated that PSR J0205+6449 has a low surface temperature and luminosity for its age of 800–5600 yrs.

Key words: stars: pulsars: general — stars: pulsars: individual: PSR J0205+6449 — X-rays: stars

1. Introduction

A neutron star (NS) is the remnant of a supernova explosion of a massive star. NSs are often observed as pulsars which emit periodic pulsed signals with a period in the typical range of $P \sim 0.001$–10 s. The short rotation period implies that NSs are compact having a mass $M_{\rm NS} \sim 1.4 M_\odot$ and a radius $R_{\rm NS} \sim 10$ km (Shapiro & Teukolsky 1986). Densities inside NSs can be very high, and the state of matter under such high densities is not yet well known (Chamel & Haensel 2008). The mass and radius of NSs (M–R relation) depend on the equation of state (EoS) of the matter (Lattimer 2012), and so measurements of $M_{\rm NS}$ and $R_{\rm NS}$ have been used to constrain the EoS and thus the state of the NS matter (e.g., Demorest et al. 2010). For a given EoS, the physical properties of the NS interior can then be inferred with several methods, one of which is to use long-term (∼Myrs) cooling trends of NSs (Yakovlev & Pethick 2004). This requires accurate measurements of the thermal radiation from NSs (pulsars) of various ages.

Radiation of pulsars is mainly observed in the radio, X-ray, and γ-ray bands (Abdo et al. 2013). The photons in these bands are believed to be produced by non-thermal processes (e.g., synchrotron and curvature radiation; Romani 1996) in the magnetosphere and thermal emission at the hot surface of a NS. The heat source for the latter could be the core (rotation-powered pulsars; RPPs), accretion (accreting X-ray binaries), or magnetic-field decay (magnetars; see Harding 2013, for a review). The surface thermal radiation is predominantly emitted in the soft X-ray band ($\leq$1 keV). Long-term and short-term variations of the thermal emission in some NSs have provided clues to the internal properties via modeling of the cooling (e.g., Brown & Cumming 2009; Viganò et al. 2013).

For accreting NSs and magnetars the depth of the heat deposition is shallow and so the thermal emission can probe the internal properties only near the surface (i.e., crusts; Cackett et al. 2013; An et al. 2018). On the contrary, the emission of some isolated RPPs is thought to be directly related to their core properties and therefore X-ray bright RPPs are of particular importance for studies of the NS core (e.g., Yakovlev & Pethick 2004). This can be done by constructing the temperature-age and/or luminosity-age trends for NSs with known ages, and by comparing the trends to NS cooling models. There are currently ∼60 NS included in such a study (e.g., Potekhin et al. 2020), but only upper-limit measurements are available for many of the NSs. Hence, larger samples and better measurements are required.

PSR J0205+6449 (J0205 hereafter) is a 65-ms RPP at a distance of 2–3.2 kpc (e.g., Roberts et al. 1993; Kothes 2013) and is the energy source of the X-ray bright pulsar wind nebula (PWN) 3C 58. The pulsar's timing behavior is complex with glitches and timing noise, but long-term observations with *RXTE* allowed a firm determination of the spin frequency (ν) and its derivative ($\dot{\nu}$). These are used to infer $B_s \approx 3 \times 10^{12}$ G, $\dot{E}_{\rm SD} = 3 \times 10^{37}$ erg s^{-1}, and $\tau_c = 5400$ yrs (e.g., Livingstone et al. 2009). The age of the pulsar is controversial; association of the PWN with the supernova SN 1181 suggested 800 yrs (Stephenson 1971) while 3000–5600 yrs were inferred from the proper motion of optical knots in the PWN (Fesen et al. 2008) or radio expansion velocity (Bietenholz 2006; Kim et al. 2019).

The emission in the central region of 3C 58 (Figure 1) is very complex with the pulsar's thermal/non-thermal and PWN components. In previous studies carried out by Slane et al. (2004) and Potekhin et al. (2020) with *Chandra* ACIS exposures, the authors used

Corresponding author: H. An

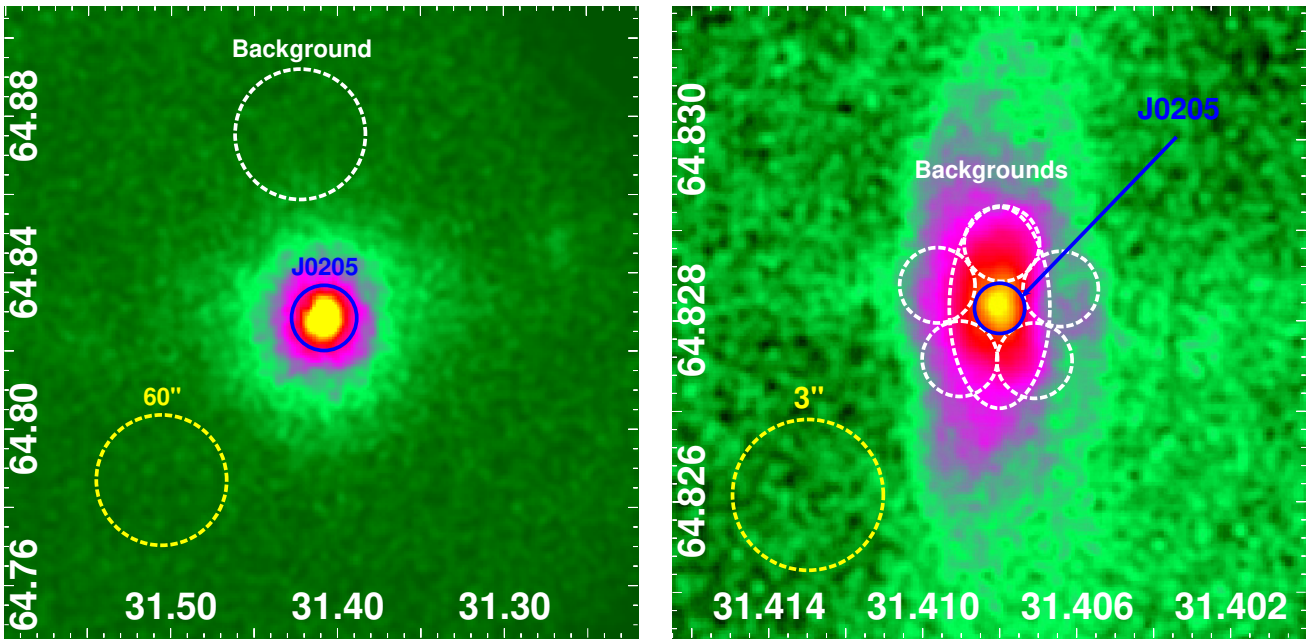

Figure 1. A 3–30 keV *NuSTAR* ($10' \times 10'$; left) and a 0.3–10 keV *Chandra* image ($0.4' \times 0.4'$; right). The images are smoothed and scales are adjusted for better legibility. Source and background regions are indicated by a blue solid circle and white dashed circles/ellipse, respectively. We use $R = 30''$ (source) and $R = 60''$ (background) apertures in the *NuSTAR* data analysis, and $R = 1''$ (source) and $R = 1.5''$ (background) apertures in the *Chandra* data analysis. A yellow dashed $R = 60''$ or $R = 3''$ circle is shown in the lower left corner of each panel for reference.

NS atmosphere-plus-power-law models and inferred the surface temperature to be $T_\infty \leq 1$ MK or 0.6 MK. This implies that for the age range of 800–5600 yrs J0205 is cold compared to other pulsars of similar ages and compared to predictions of modified-Urca-dominated cooling models. However, it is unclear whether a single power law indeed represents the pulsar's non-thermal magnetospheric emission and the PWN contamination since they have very different characteristics (e.g., $\Gamma_{\rm psr} \approx 1.1$ *vs.* $\Gamma_{\rm pwn} \approx 2$; Kuiper et al. 2010; An 2019); this might have affected the measurements and needs a careful investigation. Because the pulsar J0205 may be an important outlier in NS cooling scenarios and can give us new insights into NS interiors, a careful reanalysis of the *Chandra* data along with improved characterizations of the non-thermal X-ray emission from the pulsar and the PWN is needed.

In this paper, we analyze *NuSTAR* data of J0205 to measure its non-thermal emission. We then scrutinize archival *Chandra* data using the *NuSTAR*-inferred magnetospheric (non-thermal) contamination. We present the observational data used in this work in Section 2 and measure *NuSTAR* and *Chandra* spectra of the pulsar J0205. The *Chandra* spectra are fit with NS thermal emission models, and the results are compared with previous ones (Section 3). We then discuss implications of our measurements and conclude in Section 4.

2. OBSERVATIONS AND DATA REDUCTION

We use archival *NuSTAR* (Harrison et al. 2013) data taken in 2018 (obsid 30301011001). The data are processed with `nustardas` v1.9.0 integrated in HEASOFT v6.27 along with the calibration database 20200526 (Madsen et al. 2015). We use default event-selection criteria except for the `saamode` flag. We set it to `optimized` or `strict` as recommend by the *NuSTAR* SOC; these two settings give almost the same results and so we use the former to achieve slightly longer exposure times.

We also use archival *Chandra* data (obsids 3832, 4382, and 4383) taken in 2003 with a summed exposure time of 350 ks (Slane et al. 2004). The observations used the ACIS-S 1/2 subarray mode, and hence the timing resolution ~1.62 s is insufficient for a pulsar timing study. Therefore, the data are used only for pulsar spectral analyses. We reprocess the data using the `chandra_repro` tool in CIAO 4.12 (Fruscione et al. 2006) along with CALDB 4.9.1.

3. DATA ANALYSIS

Like for other hard X-ray bright RPPs (Kuiper & Hermsen 2015), the X-ray emission of J0205 is dominated by the pulsed magnetospheric non-thermal flux. So the best way of detecting and measuring the thermal emission is to take the pulsar's "off-pulse" interval in which the non-thermal emission is weak. *NuSTAR* does have sufficient timing resolution to resolve the 65-ms pulsation but cannot measure the <1 keV thermal emission. Furthermore, *NuSTAR*'s angular resolution (An et al. 2014) is not good enough to minimize the bright PWN background. So we have to rely on *Chandra*'s low-energy sensitivity and superb angular resolution for this study. However, *Chandra* does not provide sufficient timing resolution to resolve the pulsation. Therefore, we need to use both observatories jointly. We first characterize

the pulsar's magnetospheric emission with *NuSTAR* in the "on-pulse" interval, and then use the results to fit the *Chandra* (on and off combined) spectra.

A previous study (Kuiper et al. 2010) appears to provide a good description of the "on-pulse" emission properties ($\Gamma_{\rm psr} = 1.06(3)$, $F_{2-30\ \rm keV} = 10.7(2) \times 10^{-13}$ erg cm^{-2} s^{-1}), but the measurements were done with *RXTE* which does not have focusing capability and may suffer from calibration issues (e.g., Courvoisier et al. 2003; Weisskopf et al. 2010; Tsujimoto et al. 2011). We therefore use the *NuSTAR* data to verify the *RXTE* results and update the characterizations of the "on-pulse" spectrum.

3.1. *NuSTAR* Timing Analysis

We first perform a timing analysis with the *NuSTAR* data. We extract source and background events using circular $R = 30''$ and $R = 60''$ apertures, respectively (Figure 1 left), and apply barycenter correction to the arrival times using the radio pulsar position R.A.=02$^{\rm h}$05$^{\rm m}$37$^{\rm s}$.92 and Dec.=+64°49′41″.3 (Bietenholz et al. 2013). Since a timing solution for the same data was reported previously (An 2019), we can use the solution for our study. However, for an accurate determination of the on-pulse spectrum, we attempt to update the previous solution using the up-to-date timing calibration file 20100101v102.

For this, we perform two-dimensional (ν and $\dot{\nu}$) grid searches around the reported spin frequency $\nu = 15.20102356$ s^{-1} and its time derivative $\dot{\nu} = -4.4 \times 10^{-11}$ s^{-2} at the reference epoch MJD 58252.483104978 employing the H test (de Jager et al. 1989), and find ν=15.20102357(9) s^{-1} and $\dot{\nu} = -4.5(1) \times 10^{-11}$ s^{-2}; the second frequency derivative $\ddot{\nu}$ is not required by the data. Our results are fully consistent with the previous one.

While the solution appears to describe well the timing data of J0205 over the observation period (Figure 2), the pulsar exhibited very complex temporal behavior in the past (e.g., Livingstone et al. 2009) and so a short-term timing anomaly (e.g., glitch that can suddenly change the arrival phases on a time scale of hours to days) might have occurred during the *NuSTAR* observation. Since this may be a concern in the phase-resolved spectral analysis (Section 3.2), we further investigate the timing properties on short time scales. We split the data into twelve parts and carry out a semi-phase-coherent analysis using an asymmetric Lorentzian function as a template (Figure 2; see Kim & An 2019, for an example of the semi-phase-coherent method). A pulse profile is constructed in each time interval, and we fit the profile with the template function using the maximum likelihood method. We then measure the phase shift of the brighter first peak (P1) for each interval and find that the above timing solution does not leave any residual trend (Figure 2 bottom), meaning that the solution obtained by the grid search is valid throughout the observation period and there is no significant short-term timing anomaly in the data. We use this timing solution to facilitate a phase-resolved spectral analysis.

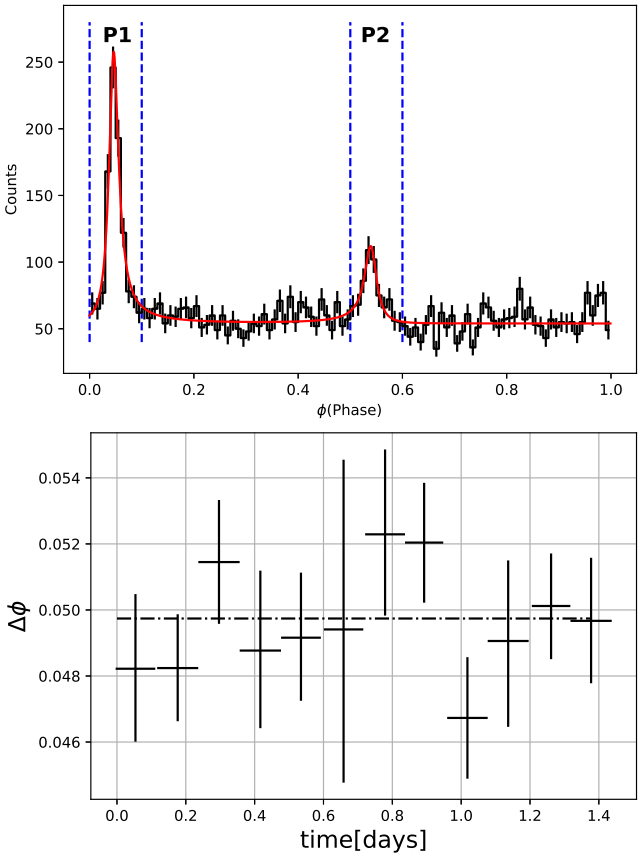

Figure 2. *Top:* A background-subtracted 3–79 keV *NuSTAR* pulse profile of PSR J0205+6449 over the 120-ks exposure. The red solid line shows the best-fit asymmetric Lorentzian template, and vertical blue dashed lines denote the on-pulse phases for the first (P1) and the second peak (P2). *Bottom:* Phase shifts of P1 over the observation time. The horizontal black dot-dashed line marks the reference phase for P1.

3.2. *NuSTAR* Spectral Analysis: On-pulse Spectrum

Because the non-thermal nature of the on-pulse spectrum of J0205 clearly demonstrates that the flux in the bright on-pulse intervals (P1 and P2; blue dotted lines in the top panel of Figure 2) is dominated by the pulsar's magnetospheric emission (Kuiper et al. 2010), we characterize it using the *NuSTAR* data in the on-pulse intervals. We select events within the $R = 30''$ source region (Figure 1) and a phase interval $\Delta\phi = 0.1$ for each of P1 and P2, and construct the source spectra. The background was extracted in the same region as that for the source over the "off-pulse" intervals. Corresponding response files are computed with the `nuproducts` tool. Because there are not enough counts in the source spectra, we bin the spectra to have at least five events per spectral bin and employ the l-statistic (Loredo 1992) in XSPEC.

We fit the spectra of P1, P2, and P1+P2 with absorbed power-law (PL) models holding the hydrogen column density ($N_{\rm H}$) fixed at 4.5×10^{21}cm^{-2} which is obtained by the pulsar and PWN spectral analyses (Slane et al. 2004; An 2019) and is similar to the Galactic value

Table 1
Best-fit parameters for the *NuSTAR* on-pulse spectra

Parameter	Flux[a] (10^{-13} erg cm^{-2} s^{-1})	$\Gamma_{\rm psr}$	χ^2/dof
P1	5.2(5)	1.0(2)	9/10
P2	1.6(4)	0.8(6)	4/7
P1+P2	7.3(6)	1.1(2)	10/16

[a] 2–30 keV flux.

of 4.8×10^{21} cm^{-2} inferred from H I measurements in the direction of J0205;[1] this has no significant influence on the >3keV *NuSTAR* spectral fits. We use this $N_{\rm H}$ value throughout this paper unless noted otherwise (see Section 3.3.5).

The fits are acceptable and the results are summarized in Table 1. We verified that changing the size of the extraction region (e.g., $R = 40 - 50''$ does not alter the results significantly. The PL indices of the two peaks are consistent with each other, and the first peak P1 is ∼3.3 times brighter than the second peak P2. The spectral index for P1+P2 is almost the same as that obtained previously with *RXTE* (Kuiper et al. 2010), but the flux value is 30–40% lower. This seems to indicate some cross-calibration issues; *RXTE*-measured spectral indices agreed very well with those measured by other instruments, but the fluxes were higher by 20–30% in previous cross-calibration studies (e.g., Courvoisier et al. 2003; Weisskopf et al. 2010; Tsujimoto et al. 2011).

3.3. *Chandra* Spectral Analysis

Because *NuSTAR* is not sensitive to the pulsar's low-energy thermal emission ($\leq$1 keV), we have to use the *Chandra* data for a determination of the thermal spectrum. The X-ray emission of J0205 and 3C 58 is very strong, and so the photons may pile up in the high-resolution *Chandra* data. In order to check this, we produce a pile-up map using the `pileup_map`[2] tool and find that the pile-up fraction at the position of the pulsar is ≈10%. Hence, it is important to take into account the pile-up effect in the spectral analysis.

We use a circular $R = 1''$ aperture to extract the source spectrum and an $R = 1.5''$ aperture north to the source region for the background (Figure 1 right). We bin the source spectra to have at least 15 events per bin and compute the response files using the `specextract` tool. As mentioned in Section 3, the spectrum observed at the pulsar position includes multiple components: the pulsar's thermal and non-thermal radiation, and the PWN emission. The pulsar's non-thermal spectrum can be approximated by the on-pulse spectrum we obtained using the *NuSTAR* data (Section 3.2), and the PWN emission can be minimized by properly selecting the background region near the pulsar. However, there can still be weak non-thermal emission in the off-pulse intervals, and the PWN background in the source region may be different from that in the surroundings (An 2019). These may leave some residual (unmodeled) contamination in the source spectrum. We therefore add a power law to the spectral model in order to fit the possible residuals.

For the complex *Chandra* spectra, we use three model components: thermal radiation, the pulsar's magnetospheric PL emission, and residual PL contamination. Note again that the last one is to mitigate the effects of inaccurate magnetospheric modeling and incomplete PWN background subtraction. The thermal radiation of the pulsar is investigated using three models: the blackbody (`bbodyrad`), neutron star atmosphere (`nsa`; Pavlov et al. 1995), and neutron star with magnetic atmosphere (`nsmaxg`; Ho et al. 2008) models in XSPEC; they were used in previous studies (Slane et al. 2004; Potekhin et al. 2020). In addition, we use the Galactic absorption (`tbabs`) and the pileup (`pileup`[3]; Davis 2001) models; for the latter we use the default parameters except for the grade morphing parameter α (e.g., see Reis et al. 2014, for a use of the pile-up model).

In summary, the spectral model for the *Chandra* data is `pileup`×`tbabs([bbodyrad, nsa or nsmaxg]+pow+pow)` of XSPEC with the parameters for the first PL (pulsar magnetosphere) being held fixed at the optimized values of the *NuSTAR* fit for P1+P2. We use $M_{\rm NS} = 1.4\,M_\odot$, $R_{\rm NS} = 10$ km, and D=2 kpc as default values when they are needed as inputs of models (`nsa` and `nsmaxg`), but change them to compare with previous results and to make sensitivity checks (Section 3.3.5). The fit results are presented in Table 2, and we summarize the individual thermal modelings below.

3.3.1. *Fit Without a Thermal Model*

We first fit the *Chandra* spectra without a thermal model (i.e., `pileup*tbabs(pow+pow)`) and find $\Gamma = 2.42(4)$ with χ^2/dof = 743/765. Although the model is formally acceptable, it is inferior to the others with a thermal component (i.e., larger χ^2/dof; Table 2). Furthermore, this model appears to be significantly softer than those of the adjacent PWN ($\Gamma_{\rm pwn} \approx 2$; An 2019), meaning that there is an excess of low-energy photons in the pulsar's spectra. The small excess can be seen in the fit residual which is displayed in Figure 3 (top left).

3.3.2. *Blackbody Model*

Blackbody emission from a hot spot can arise from magnetospheric return current and may not well represent the thermal energy originating from the core. Thus a blackbody model may not be adequate for our purpose of studying NS internal properties. Nevertheless, we use the blackbody model in order to compare with previous studies which inferred upper limits of the surface temperature (Slane et al. 2004).

We use the `pileup*tbabs*(bbodyrad+pow+pow)` model to fit the spectra. From the fit, we measure $kT = 0.15(1)$ keV and $R_{\rm BB} = 1.4(3)$ km. An F-test

[1] https://heasarc.gsfc.nasa.gov/cgi-bin/Tools/w3nh/w3nh.pl
[2] https://cxc.harvard.edu/ciao/ahelp/pileup_map.html
[3] https://heasarc.gsfc.nasa.gov/xanadu/xspec/manual/XSmodel\Pileup.html

Table 2
Best-fit results obtained from the *Chandra* spectral analysis

Model[a]	α	kT/T_∞^{b} (keV/MK)	$L_{\rm th}$ (10^{32} erg s^{-1})	Γ^{c}	Flux[c] (10^{-13} erg cm^{-2} s^{-1})	χ^2/DOF	$L_{\rm th}/L_{\rm PSR,PL}$[d]
None	0.82(12)	···	···	2.42(4)	9.9(2)	743/765	···
`bbodyrad`	0.33(16)	0.15(1)	1.2(4)	2.08(9)	9.9(2)	727/763	0.34
`nsa`	0.37(16)	0.66(3)	2.4(4)	2.12(9)	10.0(2)	733/764	0.69
`nsmaxg`	0.63(16)	0.58(7)	1.4(6)	2.24(14)	9.5(5)	738/764	0.4

The parameters $N_{\rm H} = 4.5 \times 10^{21}$ cm^{-2}, $R_{\rm NS} = 10$ km, $M_{\rm NS} = 1.4 M_\odot$, and $D = 2$ kpc are held fixed. The numbers in brackets are 1σ uncertainties at the corresponding digit.
[a] The thermal component of the `tbabs×pileup([bbodyrad,nsa,nsmaxg]+pow+pow)` model.
[b] kT (keV) for the `bbodyrad` model, and T_∞ (MK) for the `nsa` and `nsmaxg` models.
[c] Photon index and flux of the residual PL component in the 0.5–10 keV band.
[d] $L_{\rm PSR,PL}$: Magnetospheric power-law luminosity in the 0.5–30 keV band for an assumed distance at 2 kpc (see Table 3).

comparison with the 2PL model suggests that the thermal model is required with a false alarm probability of $p = 2.5 \times 10^{-4}$. The measured spectrum is shown in Figure 3 (top right). Using a distance of 3.2 kpc for a comparison with previous results ($kT = 0.15$ keV and $R_{\rm BB} = 2.6$ km; Slane et al. 2004) only changes the radius to 2.3(5) km.

3.3.3. `nsa` *Model*

The atmosphere of a neutron star may modify the surface blackbody radiation (e.g., Pavlov et al. 1995; Ho et al. 2008), and several atmospheric models have been developed and used for measuring surface emission properties of NSs. Here we consider the hydrogen atmosphere model `nsa` implemented in XSPEC. The model has the effective temperature and distance as fit parameters for given (grid) values of the neutron star's radius, mass, and magnetic-field strength. For the fits, we use the default parameters (see above) and $B_s = 10^{12}$ G.

This model improves the 2PL model (Section 3.3.1) significantly with an F-test false alarm probability of 1.2×10^{-3}, and the best-fit parameter values are $T_\infty = 0.67(3)$ MK and a thermal luminosity $L_{\rm th} = 2.4(4) \times 10^{32}$ erg s^{-1}. The measured spectrum is displayed in Figure 3 (bottom left). To compare with previous results which were obtained with an assumed distance of D=3.2 kpc, we fit the spectra using this distance value and find $T_\infty = 0.80(4)$ MK and luminosity $L_{\rm th} = 4.9(8) \times 10^{32}$ erg s^{-1}. Note that the value of T_∞ we measure is consistent with the previous result of $T_\infty \leq 1$ MK (Slane et al. 2004).

3.3.4. `nsmaxg` *Model*

We fit the spectra with another atmosphere model `nsmaxg` of XSPEC. The model assumes magnetized hydrogen in the atmosphere and optimizes the effective temperature for given radius, mass, and distance values. We use the 123100 model[4] which assumes NS properties similar to those of J0205 and was used in a previous study.

From the fit, we find $T_\infty = 0.58(7)$ MK and $L_{\rm th} = 1.4(6) \times 10^{32}$ erg s^{-1}. Although the fit is better than for 2PL only marginally (F-test false alarm probability of 2.6×10^{-2}), we further investigate this model below because it is physically motivated. The measured spectrum is presented in Figure 3 (bottom right). Potekhin et al. (2020) used the same parameters for distance and $M_{\rm NS}$ as our default values but a larger $R_{\rm NS} = 13$ km, and obtained $T_\infty = 0.57(5)$ MK and $L_{\rm th} = 1.9(6) \times 10^{32}$ erg s^{-1}; we find the same results in our fits with $R_{\rm NS} = 13$ km.

3.3.5. *Stability of Model Results*

The models discussed above provides clues about the thermal emission in J0205, but the results may depend on the model assumptions: the contamination model (i.e., pulsar magnetosphere), background (PWN), and the assumed parameter values (e.g., $M_{\rm NS}$, $R_{\rm NS}$, D, $N_{\rm H}$) of the fits. These need to be carefully investigated to make a reliable analysis of the thermal emission possible. In this section, we check how our results vary depending on these assumptions within the `nsa` and `nsmaxg` models.

We first vary the *NuSTAR*-measured magnetospheric model within the allowed range given by the 1-σ uncertainties: flux by ∼10% and the spectral index by ±0.16 (Table 1). These change the inferred T_∞ and $L_{\rm th}$ less than 10%.

We next investigate the effect of PWN background selection using the six background regions shown in Figure 1 and additional annular regions with $R_{\rm in} = 1''$ and $R_{\rm out}$ =2–5″. In this study, we find that T_∞ and $L_{\rm th}$ vary only <5% in either model. This variation is small because the background is fairly uniform in the vicinity of the pulsar, and a small nonuniformity can be accommodated in the second PL of the model.

Finally we explore effects of the model input parameters. Because the radius and mass of J0205 are not well known, we use a recent measurement of $R_{\rm NS}$ (12–14 km; Miller et al. 2019) and typical values for $M_{\rm NS}$ (1.4–1.6$M_\odot$; Özel & Freire 2016). We also vary the distance to J0205 (D=2–3.2 kpc; Roberts et al. 1993; Kothes 2013), and $N_{\rm H}$ within a range (0.45–0.5×10^{22} cm^{-2}) inferred from PWN modelings and Galactic H I measurements. We find that these induce large variation to $T_\infty/L_{\rm th}$ of 13/43% and 3/17% for the `nsa` and `nsmaxg` model, respectively. The results are presented in Table 3.

[4] https://heasarc.gsfc.nasa.gov/xanadu/xspec/manual/node202.html

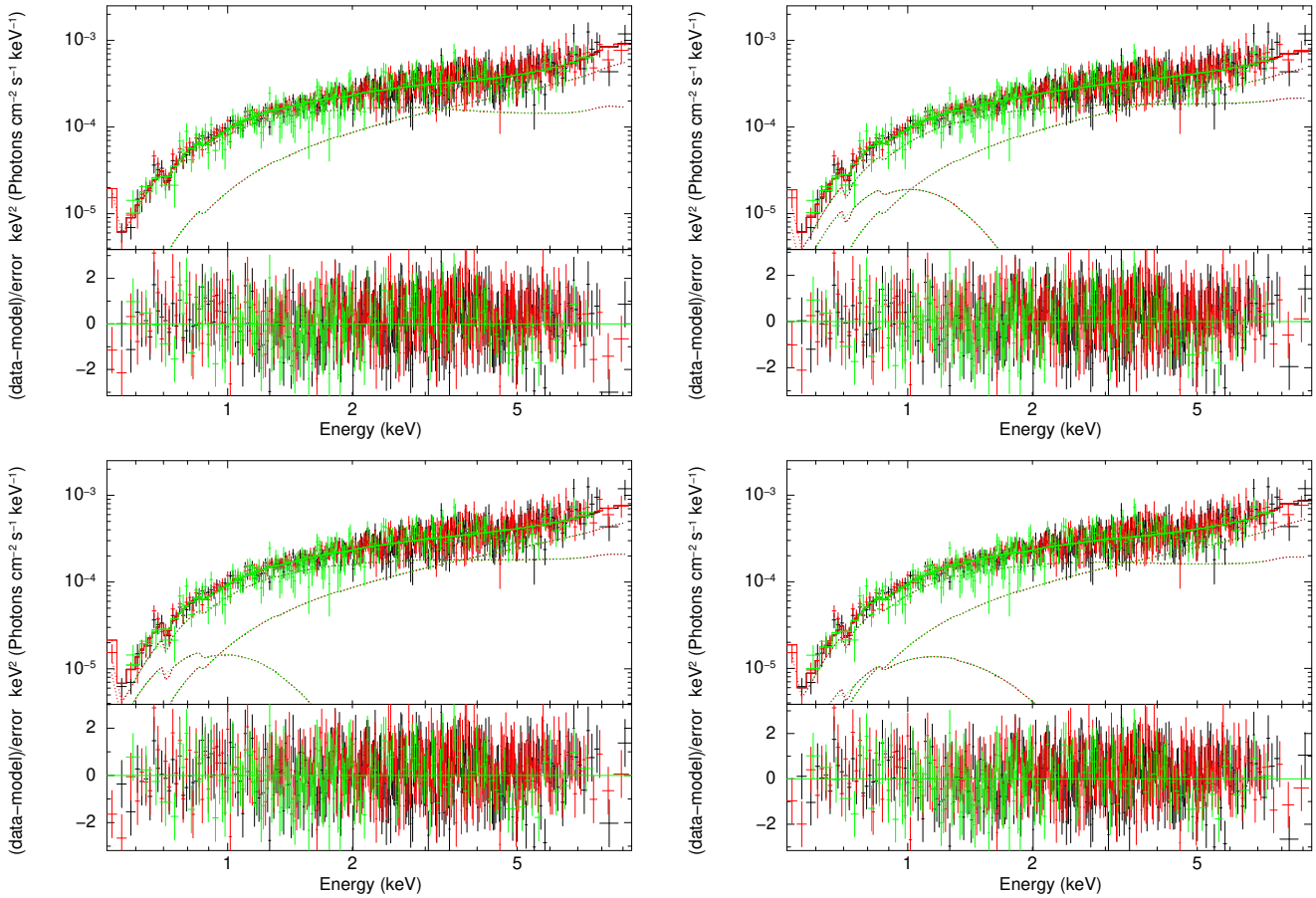

Figure 3. *Chandra* spectra and the best-fit models described in Sections 3.3.1–3.3.4. A model without a thermal component (i.e., 2PL) is displayed in the top left plot. The other panels show models with a thermal component: `bbodyrad` (top right), `nsa` (bottom left), `nsmaxg` (bottom right). See Table 2 for the parameters. The bottom diagram in each panel shows the fit residual.

In summary, for the above variations the min-max ranges for T_∞ are 0.5–0.8 MK and 0.5–0.6 MK, and the ranges for $L_{\rm th}$ are 1–5$\times10^{32}$ erg s^{-1} and 1–2 $\times10^{32}$ erg s^{-1} for the `nsa` and `nsmaxg` models, respectively.

4. SUMMARY AND DISCUSSION

We used archival *NuSTAR* and *Chandra* data to measure the X-ray properties of the pulsar PSR J0205+6449. We measured the pulsar's timing properties $\nu = 15.20102357(9)$ s^{-1} and $\dot\nu = -4.5(1)\times10^{-11}$ s^{-2} and verified that there was no strong short-term timing anomaly in the data. This timing solution was used to select the on-pulse intervals in which the pulsar's non-thermal magnetospheric emission could be best characterized, and we found that the emission was well described by a hard PL with $\Gamma_{\rm psr} = 1.1(2)$ and $F_X = 7.3(6)\times10^{-13}$ erg cm^{-2} s^{-1}. The *Chandra* spectra of the pulsar, which include both thermal and magnetospheric emission, were then modeled by a thermal+magnetosphere (on-pulse; fixed)+residual PL model. For the thermal emission we tried three different models and confirmed that J0205 has a low temperature and luminosity.

The *NuSTAR*-measured on-pulse spectrum of J0205 has 30–40% smaller flux than a previously reported value of $10.7(2)\times10^{-13}$ erg cm^{-2} s^{-1}. While this may indicate a change in the pulsar emission, variability in X-ray emission of RPPs on a time scale of ∼10 year has not been observed. Hence, we speculate that the difference is likely due to calibration uncertainties. The flux calibration uncertainty of *NuSTAR* is estimated to be at the ∼ 10% level (Madsen et al. 2015), and fluxes measured by the non-imaging instrument *RXTE* were 20–30% higher than those of other imaging observatories (Courvoisier et al. 2003; Weisskopf et al. 2010; Tsujimoto et al. 2011). So the discrepancy can be explained by cross-calibration uncertainties of the instruments. Then, the *NuSTAR* results, albeit with larger statistical uncertainties, may be better to be used in the *Chandra* data fits. This is further verified by the fact that using the *RXTE*-measured PL in the *Chandra* fits results in $\alpha = 0$, which is unrealistic.[5] This is probably because the magnetospheric PL accounts for most of the observed flux and leaves only little for the other spectral components

[5] https://cxc.harvard.edu/ciao/download/doc/pileup_abc.pdf

Table 3
Results of the stability tests

Property	nsa		nsmaxg	
	T_∞	$L_{\rm th}$	T_∞	$L_{\rm th}$
NuSTAR PL model	1.5	5.9	1.9	7.8
Background selection	0.4	1.7	1.1	4.5
Fit assumptions	13.4	43.4	2.7	17.0
Total	13.5	43.8	3.5	19.2

All numbers are 1σ percentage variations.

when the PL parameters are held fixed at the "high-flux" *RXTE* values.

Previous efforts to measure the thermal emission of J0205 were made using the same *Chandra* data but with a "single" PL model to account for the pulsar magnetospheric and residual PWN contamination. Slane et al. (2004) used a blackbody+PL and a `nsa`+PL, and concluded that T_∞ is less than 1 MK for J0205. Recently Potekhin et al. (2020) used a `nsmaxg`+PL model and inferred $T_\infty = 0.57\times10^6$ K and $L_{\rm th} = 1.9\times10^{32}$ erg s^{-1} for D=2 kpc, $M = 1.4M_\odot$, and $R_{\rm NS} = 13$ km. The PL index for the latter was not reported, but $\Gamma = 1.78^{+0.02}_{-0.04}$ inferred by the former differs significantly from $\Gamma_{\rm pwn}\approx 2$ of the adjacent PWN, meaning that there is additional hard PL contamination perhaps due to the pulsar magnetospheric emission or pileup.

We therefore used an additional (frozen) PL for the pulsar magnetosphere which was measured by our *NuSATR* data analysis. PL fits for the residual contamination in the *Chandra* spectral analysis (Section 3.3) gave $\Gamma\approx 2$ (Table 2) which is consistent with that of the PWN, thereby further justifying our use of the fixed magnetospheric PL. Our investigations of the thermal emission of J0205 with thermal+2PL models found that it has low temperature and luminosity. Although our results do not alter the previous conclusion, we argue that using two separate PLs for the spectrally distinct emissions ($\Gamma_{\rm psr} = 1.1$ for magnetosphere vs. $\Gamma_{\rm pwn}\approx 2$ for PWN residual), as we did in this work, is more adequate for characterizing the faint thermal emission.

We further checked the stability of our results (Section 3.3.5) and found that the inferred T_∞ and $L_{\rm th}$ can substantially vary depending on the assumptions (e.g., D, $R_{\rm NS}$, $M_{\rm NS}$, $N_{\rm H}$, etc). We explore possible ranges for T_∞ and $L_{\rm th}$ of J0205 and find the min-max ranges to be $T_\infty = 0.5$–0.8 MK and $L_{\rm th} = 1$–5×10^{32} erg s^{-1}. These variations do not change the previous conclusion derived from the cooling models that neutrino cooling via the modified Urca mechanism alone is insufficient to explain the low temperature and luminosity inferred for J0205 (e.g., Slane et al. 2004). However, our analyses make the conclusion more robust in that we showed that different handling of the pileup, backgrounds, and contamination of the magnetosphere/PWN results in similarly low temperature and luminosity.

Nevertheless, there is still large unexplored parameter space in the determination of the surface thermal emission of J0205, and hence the above results need to be regarded as representative ranges. The magnetic inclination angle and chemical composition in the atmosphere are still unknown; these can change the emission properties (e.g., Mori and Ho 2007). Accurate characterization of the non-thermal contamination is also important. A weaker magnetospheric emission may increase the temperature and luminosity, although this is not very likely given that the measured X-ray spectra do not show a prominent thermal bump at low energies (Figure 3). Larger fluxes in the PL components would do the opposite; the inferred temperature and luminosity would decrease. In addition, if the low-energy X-ray emission is mainly produced in hot polar caps by return current, the surface temperature and luminosity (heat from the core) could be even smaller. These effects require further theoretical and observational studies.

There are only a few sources with very low T_∞ and $L_{\rm th}$ for their ages, and finding more will be very intriguing as they provide information on the internal properties of NSs. Possible candidates are the so-called "soft γ-ray pulsars" (including J0205; Kuiper & Hermsen 2015) which exhibit strong power-law emission in the X-ray to soft γ-ray band. They seem not to emit significant thermal radiation and hence may have very low temperatures and luminosities, like J0205. Their ages span a wide range (τ_c =1–43 kyr), and thus these pulsars can be very useful to constrain the cooling models and internal properties of NSs. Observations of soft gamma-ray pulsars with *Chandra*, *NuSTAR* and future X-ray observatories will help to make a step forward in understanding NS internal properties. Because soft γ-ray pulsars have strong magnetospheric emission (and often a bright PWN, e.g., PSR J1418−6058; Kim & An 2020), our approach of separately modeling the magnetosphere will be useful.

Acknowledgments

We thank the anonymous referees for their careful reading of the paper and insightful comments. This research was supported by the Basic Science Research Program through the National Research Foundation of Korea (NRF) funded by the Ministry of Science, ICT & Future Planning (grant no. NRF-2017R1C1B2004566).

References

Abdo, A. A., Ajello, M., Allafort, A., et al. 2013, The Second Fermi Large Area Telescope Catalog of Gamma-Ray Pulsars, ApJS, 208, 17

An, H., Madsen, K. K., Westergaard, N. J. et al., 2014, In-flight PSF Calibration of the NuSTAR Hard X-ray Optics, SPIE, 9144, 91441Q

An, H., Cumming, A., & Kaspi, V. M. 2018, Flux Relaxation after Two Outbursts of the Magnetar SGR 1627-41 and Possible Hard X-Ray Emission, ApJ, 859, 16

An, H. 2019, NuSTAR Hard X-Ray Studies of the Pulsar Wind Nebula 3C 58, ApJ, 876, 150

Bietenholz, M. F. 2006, Radio Images of 3C 58: Expansion and Motion of Its Wisp, ApJ, 645, 1180

Bietenholz, M. F., Kondratiev, V., Ransom, S., et al. 2013, The Proper Motion of PSR J0205+6449 in 3C 58, MNRAS, 431, 2590

Brown, E. F., & Cumming, A. 2009, Mapping Crustal Heating with the Cooling Light Curves of Quasi-Persistent Transients, ApJ, 698, 1020

Cackett, E. M., Brown, E. F., Cumming, A., et al. 2013, A Change in the Quiescent X-Ray Spectrum of the Neutron Star Low-mass X-Ray Binary MXB 1659-29, ApJ, 774, 131

Chamel, N., & Haensel, P. 2008, Physics of Neutron Star Crusts, LRR, 11, 10

Courvoisier, T. J.-L., Beckmann, V., Bourban, G., et al. 2003, Simultaneous Observations of the Quasar 3C 273 with INTEGRAL and RXTE, A&A, 411, L343

Davis, J. E. 2001, Event Pileup in Charge-coupled Devices, ApJ, 562, 575

Demorest, P. B., Pennucci, T., Ransom, S. M., et al. 2010, A Two-solar-mass Neutron Star Measured Using Shapiro Delay, Nature, 467, 1081

de Jager, O. C., Raubenheimer, B. C., & Swanepoel, J. W. H. 1989, A Powerful Test for Weak Periodic Signals with Unknown Light Curve Shape in Sparse Data, A&A, 221, 190

Fesen, R., Rudie, G., Hurford, A., & Soto, A. 2008, Optical Imaging and Spectroscopy of the Galactic Supernova Remnant 3C 58 (G130.7+3.1), ApJS, 174, 379

Fruscione, A., McDowell, J. C., Allen, G. E., et al. 2006, CIAO: Chandra's Data Analysis System, SPIE, 6270, 62701V

Harding, A. K. 2013, The Neutron Star Zoo, Frontiers Phys., 8, 679

Harrison, F. A., Craig, W. W., Christensen, F. E., et al. 2013, The Nuclear Spectroscopic Telescope Array (NuSTAR) High-energy X-Ray Mission, ApJ, 770, 103

Ho, W. C. G., Potekhin, A. Y., & Chabrier, G. 2008, Model X-Ray Spectra of Magnetic Neutron Stars with Hydrogen Atmospheres, ApJS, 178, 102

Kim, M., & An, H. 2019, Measuring Timing Properties of PSR B0540-069, JKAS, 52, 41

Kim, M., & An, H. 2020, Characterizing X-Ray Properties of the Gamma-Ray Pulsar PSR J1418-6058 in the Rabbit Pulsar Wind Nebula, ApJ, 892, 5

Kim, S., Park, J., & An, H. 2019, Investigating the Pulsar Wind Nebula 3C 58 Using Emission Models, JKAS, 52, 173

Kothes, R. 2013, Distance and Age of the Pulsar Wind Nebula 3C 58, A&A, 560, A18

Kuiper, L., Hermsen, W., Urama, J. O., et al. 2010, Hard X-ray Timing and Spectral Characteristics of the Energetic Pulsar PSR J0205+6449 in Supernova Remnant 3C 58. An RXTE PCA/HEXTE and XMM-Newton View on the 0.5-250 keV Band, A&A, 515, A34

Kuiper, L., & Hermsen, W. 2015, The Soft γ-ray Pulsar Population: A High-energy Overview, MNRAS, 449, 3827

Lattimer, J. M. 2012, The Nuclear Equation of State and Neutron Star Masses, Annu. Rev. Nucl. Part. Sci., 62, 485

Livingstone, M. A., Ransom, S. M., Camilo, F., et al. 2009, X-ray and Radio Timing of the Pulsar in 3C 58, ApJ, 706, 1163

Loredo, T. J. 1992, Promise of Bayesian Inference for Astrophysics. In: Feigelson E. D., Babu G. J. (eds) Statistical Challenges in Modern Astronomy (New York: Springer), 275

Madsen, K. K., Harrison, F. A., Markwardt, C. B., et al. 2015, Calibration of the NuSTAR High-energy Focusing X-ray Telescope, ApJS, 220, 8

Miller, M. C., Lamb, F. K., Dittmann, A. J., et al. 2019, PSR J0030+0451 Mass and Radius from NICER Data and Implications for the Properties of Neutron Star Matter, ApJL, 887, L24

Mori, K., & Ho, W. C. G. 2007, Modelling Mid-Z Element Atmospheres for Strongly Magnetized Neutron Stars, MNRAS, 377, 905

Özel, F., & Freire, P. 2016, Masses, Radii, and the Equation of State of Neutron Stars, ARA&A, 54, 401

Pavlov, G. G., Shibanov, Y. A., Zavlin, V. E., & Meyer, R. D. 1995, Neutron Star Atmospheres, NATO Adv. Sci. Inst. C, 450, 71

Potekhin, A. Y., Zyuzin, D. A., Yakovlev, D. G., et al. 2020, Thermal Luminosities of Cooling Neutron Stars, MNRAS, 496, 5052

Reis, R. C., Reynolds, M. T., Miller, J. M., & Walton, D. J. 2014, Reflection from the Strong Gravity Regime in a Lensed Quasar at Redshift $z = 0.658$, Nature, 507, 207

Roberts, D. A., Goss, W. M., Kalberla, P. M. W., et al. 1993, High Resolution H I Observations of 3C 58, A&A, 274, 427

Romani, R. W. 1996, Gamma-Ray Pulsars: Radiation Processes in the Outer Magnetosphere, ApJ, 470, 469

Shapiro, S. L., & Teukolsky, S. A. 1986, Black Holes, White Dwarfs and Neutron Stars: The Physics of Compact Objects (Hoboken, NJ: John Wiley & Sons)

Slane, P., Helfand, D. J., van der Swaluw, E., & Murray, S. S. 2004, New Constraints on the Structure and Evolution of the Pulsar Wind Nebula 3C 58, ApJ, 616, 403

Stephenson, F. R. 1971, Suspected Supernova in A.D. 1181, QJRAS, 12,

Tsujimoto, M., Guainazzi, M., Plucinsky, P. P., et al. 2011, Cross-calibration of the X-ray Instruments Onboard the Chandra, INTEGRAL, RXTE, Suzaku, Swift, and XMM-Newton Observatories Using G21.5-0.9, A&A, 525, A25

Viganò, D., Rea, N., Pons, J. A., et al. 2013, Unifying the Observational Diversity of Isolated Neutron Stars via Magneto-thermal Evolution Models, MNRAS, 434, 123

Weisskopf, M. C., Guainazzi, M., Jahoda, K., et al. 2010, On Calibrations Using the Crab Nebula and Models of the Nebular X-Ray Emission, ApJ, 713, 912

Yakovlev, D. G., & Pethick, C. J. 2004, Neutron Star Cooling, ARA&A, 42, 169